STIM1 couples to ORAI1 via an intramolecular transition into an extended conformation

Martin Muik[1,4], Marc Fahrner[1,4], Rainer Schindl[1,4], Peter Stathopulos[2], Irene Frischauf[1], Isabella Derler[1], Peter Plenk[1], Barbara Lackner[1], Klaus Groschner[3], Mitsuhiko Ikura[2] and Christoph Romanin[1,*]

[1]Institute of Biophysics, University of Linz, Linz, Austria, [2]Department of Medical Biophysics, University of Toronto, Toronto, Ontario, Canada and [3]Institute of Pharmaceutical Sciences, University of Graz, Graz, Austria

Stromal interaction molecule (STIM1) and ORAI1 are key components of the Ca^{2+} release-activated Ca^{2+} (CRAC) current having an important role in T-cell activation and mast cell degranulation. CRAC channel activation occurs via physical interaction of ORAI1 with STIM1 when endoplasmic reticulum Ca^{2+} stores are depleted. Here we show, utilizing a novel STIM1-derived Förster resonance energy transfer sensor, that the ORAI1 activating small fragment (OASF) undergoes a C-terminal, intramolecular transition into an extended conformation when activating ORAI1. The C-terminal rearrangement of STIM1 does not require a functional CRAC channel, suggesting interaction with ORAI1 as sufficient for this conformational switch. Extended conformations were also engineered by mutations within the first and third coiled-coil domains in the cytosolic portion of STIM1 revealing the involvement of hydrophobic residues in the intramolecular transition. Corresponding full-length STIM1 mutants exhibited enhanced interaction with ORAI1 inducing constitutive CRAC currents, even in the absence of store depletion. We suggest that these mutant STIM1 proteins imitate a physiological activated state, which mimics the intramolecular transition that occurs in native STIM1 upon store depletion.

*Corresponding author. Institute of Biophysics, University of Linz, 4040 Linz, Austria. Tel.: +43 732 2468 9272; Fax: +43 732 2468 9280; E-mail: christoph.romanin@jku.at
[4]These authors contributed equally to this work

Introduction

Calcium signalling in the cytosol of excitable and non-excitable cells is of crucial importance. It triggers both short-term responses like secretion, muscle contraction or metabolism and also long-term regulation including transcription, cell growth and apoptosis (Berridge *et al*, 2003). A major calcium pathway is mediated by store-operated channels (SOCs). The endoplasmic reticulum (ER) calcium stores are depleted upon binding of inositol-1,4,5-triphosphate (IP_3) to their receptors, resulting in the activation of the plasma membrane Ca^{2+} release-activated Ca^{2+} (CRAC) channels (Parekh and Putney, 2005). CRAC channels are characterized by a high Ca^{2+} selectivity and very low single channel conductance (Hoth and Penner, 1992; Parekh and Putney, 2005). Their activation enhances cytosolic Ca^{2+} levels and thereby stimulates gene expression via the nuclear factor of activated T cells, resulting in cytokine secretion in the early stages of immune responses (Feske, 2007; Oh-hora and Rao, 2008).

A systematic genetic screen by RNA interference has discovered the stromal interaction molecule (STIM1) and ORAI1 (also termed CRACM1) as the main molecular components of CRAC channels (Liou *et al*, 2005; Roos *et al*, 2005; Feske *et al*, 2006; Zhang *et al*, 2006; Vig *et al*, 2006b; Hogan *et al*, 2010). STIM1 has been identified as the ER-located Ca^{2+} sensor (Liou *et al*, 2005; Roos *et al*, 2005), which senses the luminal Ca^{2+} content by its N-terminal EF hand. ORAI1 is a Ca^{2+} selective channel located in the plasma membrane with four transmembrane segments and cytosolic N- and C-terminal strands (Prakriya *et al*, 2006; Yeromin *et al*, 2006; Vig *et al*, 2006b; Schindl *et al*, 2008). A mutation within ORAI1, that is R91W, leading to a non-functional channel has been directly linked to severe combined immune deficiency (SCID) (Feske *et al*, 2006).

At resting state, STIM1 is uniformly distributed throughout the ER membrane. Store depletion triggers STIM1 multimer formation. These aggregates then translocate into puncta close to the plasma membrane (Liou *et al*, 2005, 2007; Zhang *et al*, 2005; Baba *et al*, 2006; Luik *et al*, 2006; Mercer *et al*, 2006; Soboloff *et al*, 2006; Wu *et al*, 2006; Xu *et al*, 2006), thereby activating ORAI1/CRAC channels. Besides an EF-hand pair, the luminal N-terminus of STIM1 further contains a sterile-α motif, all these domains are required for multimerization (Stathopulos *et al*, 2008, 2009). Following a single transmembrane helix, the cytoplasmic C terminus includes three coiled-coil domains (Hogan *et al*, 2010), which overlap with an ezrin–radixin–moesin (ERM)-like domain, a serine/proline- and a lysine-rich segment (Liou *et al*, 2005; Baba *et al*, 2006; Huang *et al*, 2006; Smyth *et al*, 2006) (see also Supplementary Figure S4A). The CAD/SOAR

domain encompasses roughly aa 340–448 including the second and third coiled-coil domain and represents the smallest STIM1 C-terminal fragment that couples to and activates ORAI1 channels (Park *et al*, 2009; Yuan *et al*, 2009). An interaction between CAD and both the N- and C-terminal regions of ORAI1 has been determined by *in vitro* pull-down experiments (Park *et al*, 2009).

We and others have visualized coupling between STIM1 and ORAI1 in store-depleted cells by Förster resonance energy transfer (FRET) microscopy (Barr *et al*, 2008; Muik *et al*, 2008; Navarro-Borelly *et al*, 2008). The cytosolic C-terminal portion of ORAI1 that contains a putative coiled-coil domain couples with STIM1 (Muik *et al*, 2008; Frischauf *et al*, 2009).

In this study, we designed a STIM1 conformational sensor that demonstrates an intramolecular transition into an extended conformation when binding to ORAI1. Engineering extended conformations via mutations in coiled-coil domains facilitated STIM1 coupling to ORAI1 probably by alterations of coiled-coil intramolecular interactions. The STIM1 conformational sensor further revealed novel characteristics of the SCID-linked ORAI1–R91W mutant and the CRAC modifier 2-aminoethoxy-diphenyl-borate (2-APB) in their interactions with STIM1.

Results

A STIM1-derived conformational sensor

The conformational choreography that evokes activation of ORAI channels via their interaction with STIM1 is unclear. While intermolecular FRET measurements within an assembly of CFP- and YFP-tagged ORAI1 proteins have been carried out (Navarro-Borelly *et al*, 2008), intramolecular FRET within one ORAI1 protein might provide a more direct read-out of conformational rearrangements that occur upon coupling with STIM1. However, N- and C-terminally double-labelled ORAI1 proteins were not applicable by reason of significantly reduced plasma membrane localization (data not shown). Therefore, we focused on the development of a STIM1-derived conformational sensor that might allow for monitoring of intramolecular rearrangements within the STIM1 cytosolic portion when interacting with ORAI1. As the STIM1 C-terminus acts as a surrogate for full-length STIM1 (Huang *et al*, 2006; Muik *et al*, 2008), we initially started to generate a variety of double-labelled STIM1 C-terminal constructs of decreasing length (Figure 1) in an attempt to optimize sensor features for reporting conformational rearrangements relevant for the STIM1/ORAI coupling machinery. Focus was placed on constructs that (i) contained at least the minimal regions previously identified for the interaction with ORAI1 (Muik *et al*, 2009; Park *et al*, 2009; Yuan *et al*, 2009) and (ii) were still functional both for the coupling to as well as activation of ORAI1 channels. All constructs included the first coiled-coil region in addition to the CAD/SOAR domain. Expression of these double-labelled constructs in HEK 293 cells revealed a range of FRET values between ~ 0.9 and ~ 0.2 (Figure 1A). While showing a remarkably high maximum (~ 0.9) around our previously reported ORAI1 activating small fragment (OASF; aa 233–474), C-terminal extension up to the wild-type length (aa 685) resulted in a gradual decrease of FRET. Interestingly, fragments shorter than OASF also exhibited an attenuation of FRET (Figure 1A), indicating that construct length is not the only factor determining FRET.

Double-labelled fragments aa 233–420/430 are most likely inactive (Zhang *et al*, 2008; Muik *et al*, 2009; Park *et al*, 2009; Yuan *et al*, 2009), while 233–450 or 233–474 (OASF) and larger fragments are proposed as sufficient for interaction and ORAI1 current activation (Muik *et al*, 2009). In this study we focused on the double-labelled aa 233–474 fragment, as the former tends to form large clusters without ORAI1 co-expression (Muik *et al*, 2009; Yuan *et al*, 2009). Indeed, double-labelled YFP–STIM1–233–474–CFP (termed YFP–OASF–CFP) allowed for robust constitutive activation of ORAI1-derived currents with CRAC-like biophysical characteristics (Figure 1B). The current densities obtained with the double-labelled OASF sensor were somewhat smaller than those of its single-labelled form (Muik *et al*, 2009) pointing to a slightly reduced activation capacity and/or affinity for ORAI1. The functionality of this conformational STIM1 sensor constitutes a powerful tool to monitor intramolecular rearrangements within OASF upon binding to ORAI1 (see below).

This double-labelled YFP–OASF–CFP construct when expressed alone in HEK 293 cells mainly exhibited a uniform, cytosolic distribution and yielded remarkably high FRET (Figure 1A and C), reaching ~ 0.9, much higher than ~ 0.2 typically found in our previous experiments with single-labelled constructs detecting OASF oligomerization (Muik *et al*, 2009). YFP–OASF–CFP proteins were detected by an anti-GFP antibody as a single band in western blot corresponding to the complete sensor form without any smaller, cleaved fragments (Figure 1D). The high FRET value of YFP–OASF–CFP might result from both intramolecular and intermolecular proximity of fluorophores, representing a head-to-tail orientation and dimerization/oligomerization (Muik *et al*, 2009), respectively (Figure 1E).

In an attempt to roughly estimate intermolecular FRET, we generated additional constructs that carried identical labels (either CFP or YFP) on both N- and C-termini giving rise only to intermolecular but not intramolecular FRET (Figure 1E). Co-expressed CFP–OASF–CFP and YFP–OASF–YFP revealed smaller FRET values of ~ 0.18 (Figure 1E). Thus, the high FRET observed with the YFP–OASF–CFP conformational sensor is suggested to reflect primarily intramolecular rather than intermolecular interactions and assumedly arises from a head-to-tail proximity of fluorophores within OASF (see Figure 1E).

Conformational coupling of OASF sensor to ORAI1

The cytosolic portion of STIM1 interacts with both ORAI1 N- and C-termini (Park *et al*, 2009). The multiple interaction sites leading to ORAI1 activation might involve a conformational rearrangement within STIM1. The YFP–OASF–CFP conformational sensor enabled us for the first time to address this question. Its expression together with unlabelled ORAI1 in HEK293 cells led to a clear redistribution of the OASF sensor with partial plasma membrane as well as cytosolic targeting. The OASF FRET sensor exhibited clearly stronger membrane targeting than the double-labelled whole STIM1 C-terminus (233–685) consistent with its higher affinity to ORAI1, which was abolished with the shorter 233–430 fragment as evident from density profiles (Supplementary Figure S1). YFP–OASF–CFP yielded higher FRET in the cytosol, while significantly lower FRET was obtained with the fraction of the sensor that was targeted close to the plasma membrane
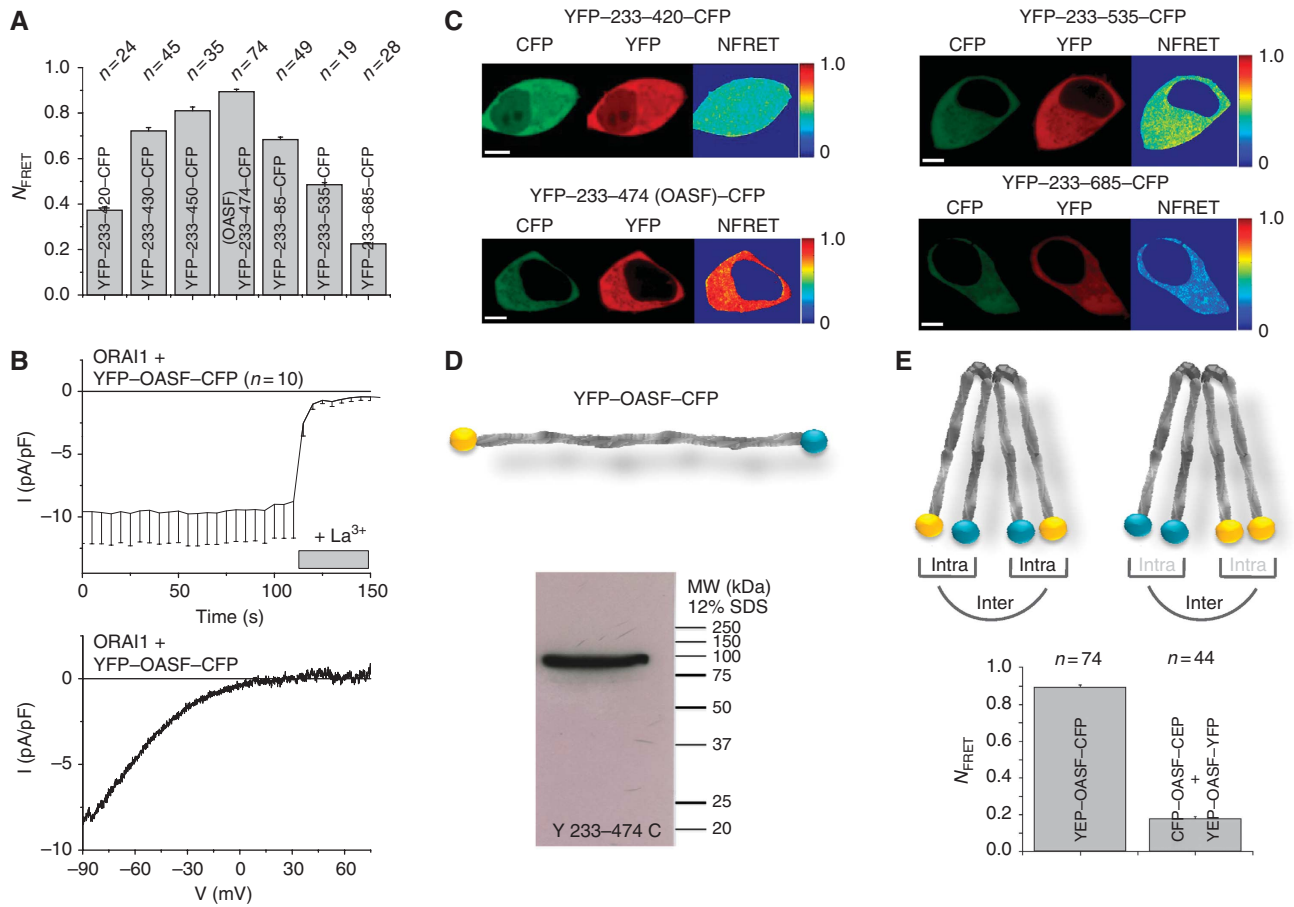
Figure 1 Designing a STIM1-derived conformational sensor. (**A**) Block diagram summarizing intermolecular/intramolecular NFRET of double-labelled YFP–STIM1–CFP fragments: 233–420, 233–430, 233–450, 233–474 (OASF), 233–485, 233–535 and 233–685 (complete STIM1 C-terminus). (**B**) Time course of constitutive whole-cell inward currents at $-86\,mV$ of HEK293 cells expressing YFP–OASF–CFP with ORAI1 (upper panel) and respective I/V curve taken at $t=0\,s$ (lower panel). (**C**) Localization and calculated NFRET life cell image series of selected STIM1 fragments: 233–420, 233–474 (OASF), 233–535 and 233–685. Calibration bar is $5\,\mu m$ throughout. (**D**) The YFP–OASF–CFP FRET sensor detected by western blot with an anti-GFP antibody when expressed in HEK293 cells. (**E**) A cartoon indicating the intramolecular/intermolecular FRET of OASF labelled either with YFP/CFP (left) or CFP/CFP, YFP/YFP (right). Block diagram comparing intermolecular with intramolecular NFRET of double-labelled STIM1 OASF fragments as depicted in the upper panel.

where ORAI1 is located (Figure 2A). This decrease of FRET was not due to a diminished intermolecular FRET, as dimerization/oligomerization of OASF when coupled to ORAI1 slightly enhances FRET as previously shown (Muik *et al*, 2009) for single-labelled and uniformly double-labelled constructs (Supplementary Figure S2A and B). Hence, our data suggest a reduction of intramolecular FRET by a rearrangement within YFP–OASF–CFP into an extended head-to-tail configuration upon its coupling to ORAI1, although an additional change in fluorophore orientation affecting FRET cannot be excluded. This decrease of FRET from the OASF conformational sensor was similarly observed upon co-expression with the non-conducting (Prakriya *et al*, 2006; Yeromin *et al*, 2006; Vig *et al*, 2006a) ORAI1–E106Q mutant (Figure 2B), indicating that it was not directly linked to Ca^{2+} entry or caused by increases in submembrane intracellular Ca^{2+} concentrations. Thus, the intramolecular transition to the extended conformation apparently resulted from OASF coupling with ORAI1 upstream of CRAC channel opening and Ca^{2+} entry. The ORAI1–L273S mutant that exhibits disrupted communication with STIM1 (Muik *et al*, 2008) consistently failed to interact with OASF conformational

sensor, displaying a rather uniform, high FRET that is similar both in cytosolic and plasma membrane adjacent regions (Figure 2C). The extended conformation of OASF when coupled to ORAI1 may reflect a specific, intramolecular transition possibly exposing the minimal region, that is CAD/SOAR (Park *et al*, 2009; Yuan *et al*, 2009), essential for this interaction with and/or gating of the ORAI1 channel (Park *et al*, 2009).

Engineering head-to-tail proximity of OASF

STIM1 encodes three putative coiled-coil domains (Hogan *et al*, 2010) within the cytosolic portion (Supplementary Figure S2A) that might contribute to the OASF conformation via intramolecular interactions. In general, coiled-coil domains are well known for mediating intermolecular as well as intramolecular protein associations via both hydrophobic and electrostatic interactions (Steinmetz *et al*, 2007; Grigoryan and Keating, 2008; Parry *et al*, 2008). In an attempt to engineer OASF in its extended conformation, we initially decreased OASF length from its N-terminal side, as CAD/SOAR is primarily devoid of the first coiled-coil domain (aa 233–342). We further mutated various hydrophobic leucines
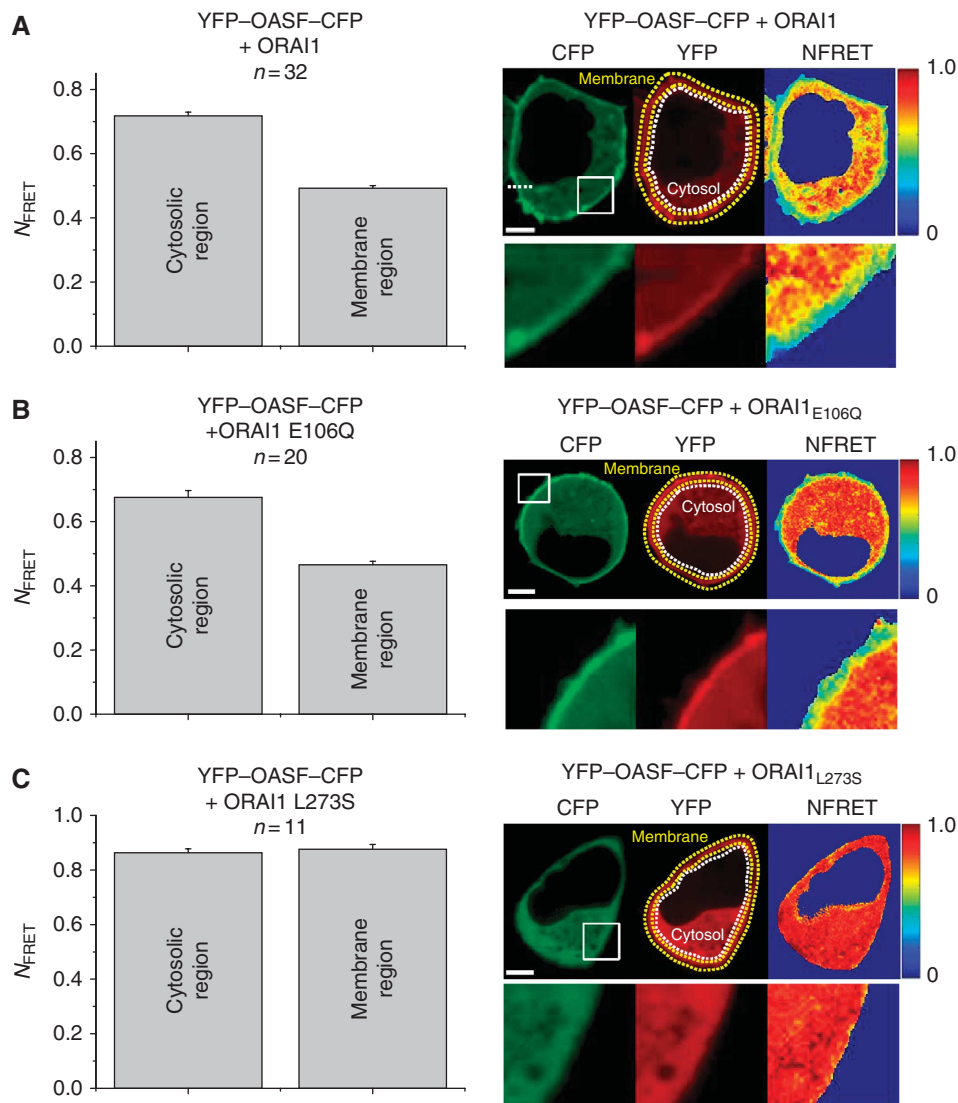
Figure 2 OASF sensor coupling to ORAI1. (Right panel) Localization and calculated NFRET life cell image series of HEK293 cells expressing YFP–OASF–CFP and (**A**) ORAI1, (**B**) ORAI1$_{E106Q}$ (**C**) ORAI1$_{L273S}$. Calibration bar is 5 µm throughout. Magnified section as indicated by the white box highlights the decrease of FRET in regions of the plasma membrane compared with the cytosol in (**A**, **B**). (Left panel) Respective block diagram of separately calculated NFRET for regions including the plasma membrane (within the two yellow borders) and the cytosol (within white border). The 'plasma membrane' was assumed as 1.5–2 µm of the edge of the cell image.

at position a or d within a heptad repeat (Woolfson, 2005) that are highly conserved between various species (Supplementary Figure S3), in an attempt to locally interfere with the putative first coiled-coil structure. Among several constructs (Supplementary Figure S4B), the very N-terminal portion (aa 233–251) appeared most interesting, as its deletion or L to S point mutations therein (L248S, L251S) led to constructs with a substantial reduction of FRET compared with the wild-type sensor (Figure 3A and C; Supplementary Figure S4B). To circumvent the impact of N-terminal truncations on FRET, we focused (below) on the OASF L251S point mutant, which assumed an extended conformation independent of interaction with ORAI1. Several other L to S mutations within the first coiled-coil downstream to aa L251 led to smaller or almost no reduction of FRET (Supplementary Figure S4B) underscoring the importance of the N-terminal region (aa 233–251) of OASF to this conformational transition. Thus, the first, putative coiled-coil

domain likely has a role in intramolecular coiled-coil associations within OASF.

To reveal an involvement of the second coiled-coil domain in the head-to-tail proximity of OASF, we engineered L373S, L373S A376S, A376K hydrophobic mutations (Frischauf *et al*, 2009; Covington *et al*, 2010) to analogously interfere with the putative coiled-coil structure. Additionally, this region has been suggested (Frischauf *et al*, 2009; Calloway *et al*, 2010; Covington *et al*, 2010) to encompass the STIM1-binding site for ORAI1, as the above mutations interfered with STIM1 coupling to ORAI1 (Frischauf *et al*, 2009; Covington *et al*, 2010). All of these YFP–OASF–CFP sensor mutants exhibited a significant reduction of FRET compared with wild type, with the A376K mutant being most pronounced (Supplementary Figure S4B; Figure 3A and C). These data suggest a contribution of the second coiled-coil domain in controlling intramolecular transitions in addition to its role as potential binding site for ORAI1.
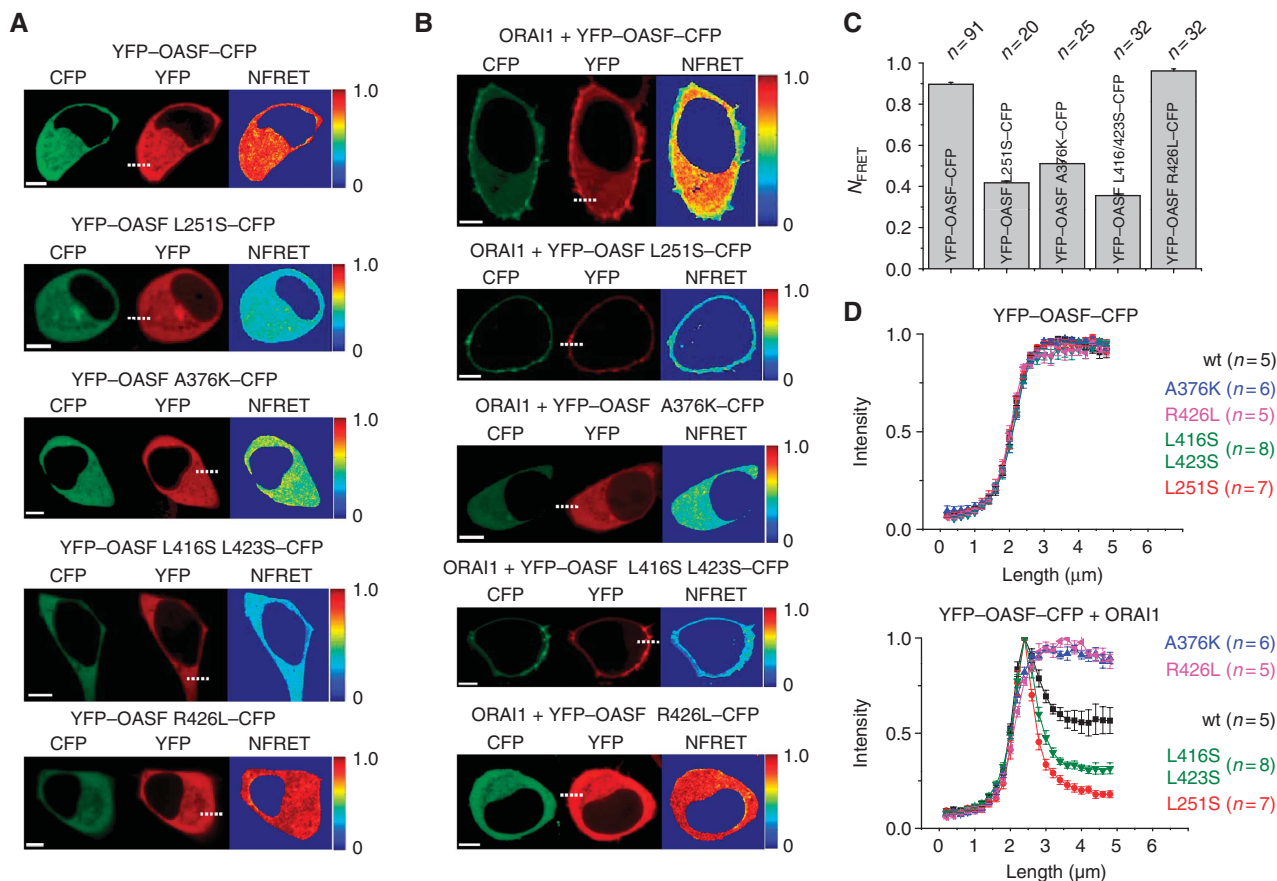
Figure 3 Engineering OASF head-to-tail proximity by mutations. (**A**, **B**) Localization and calculated NFRET life cell image series of YFP–OASF–CFP wild-type and mutants without (**A**) or with (**B**) ORAI1 co-expressed. Calibration bar is 5 μm throughout. (**C**) Block diagram summarizing NFRET of double-labelled OASF mutants: YFP–OASF–CFP (wild type), YFP–OASF L251S–CFP, YFP–OASF A376K–CFP, YFP–OASF L416S L423S–CFP and YFP–OASF R426L–CFP. (**D**) Intensity plots representing localization of YFP–OASF–CFP wild-type and mutants without (upper panel) and with (lower panel) ORAI1 in regions close to the plasma membrane as indicated by the dashed line.

The C-terminal segment of OASF around aa 420–430 might also have a role in the head-to-tail proximity based on the substantial reduction of FRET upon its deletion (see Figure 1A). In an attempt to alternatively affect head-to-tail proximity of OASF, which might be governed by intramolecular coiled-coil interactions, we aimed to potentially disrupt (L416S, V419S, L423S) or enhance (R426L) the third putative coiled-coil domain (Hogan *et al*, 2010) by introducing L/V to S or R to L mutations in this region (Gruber *et al*, 2006). All four residues are highly conserved between various species (Supplementary Figure S3). The former mutants indeed showed a significant attenuation of FRET (Supplementary Figure S4B) with the YFP–OASF L416S L423S–CFP double mutant revealing the most pronounced reduction, while the R426L OASF sensor mutant displayed a significantly higher FRET than wild type (Figure 3A and C; Supplementary Figure S4), implicating the third coiled-coil region in mediating OASF head-to-tail proximity.

In summary, the L251S, A376K and L416/423S OASF sensor mutants showed substantial FRET reduction by ∼0.4 compared with the OASF wild-type form, which likely resulted from a pronounced decrease of head-to-tail proximity. Intermolecular FRET measurements suggested comparable degree of dimerization/oligomerization of OASF and mutants (Figure 4A).

In vitro analyses of purified OASF wild-type and mutant forms provided further evidence for distinct conformations with no change in the oligomerization state (Figure 4B and C). An extended version of OASF (OASF-ext), encompassing aa 234–491 was used in the *in vitro* analyses because this protein was less susceptible to degradation in *Escherichia coli* cells. Wild-type, L251S, L416S and L423S OASF-ext proteins were attainable at > 95 % purity (Figure 4B, inset). All four of the recombinant proteins showed a high α-helicity, assessed by far-UV circular dichroism (CD), typical of coiled-coil motifs. Interestingly, all three mutant forms exhibited more pronounced negative ellipticity (i.e. see 208 and 222 nm) compared with wild type (Figure 4B). These spectral changes probably reflected a conformational change rather than an increased α-helical content, since the thermal melts of the mutant proteins, measured at 222 nm, did not show an enhanced stability expected to accompany increased levels of secondary structure compared with wild type (Supplementary Figure S5). A similar phenomenon occurs with calmodulin, which displays enhanced negative ellipticity in the far-UV CD spectra in response to Ca^{2+} binding (Martin and Bayley, 1986) without a change in helical content, but rather a conformational rearrangement of the secondary structure elements in three-dimensional space (Finn *et al*, 1995). Consistent with a mutation-induced conformational
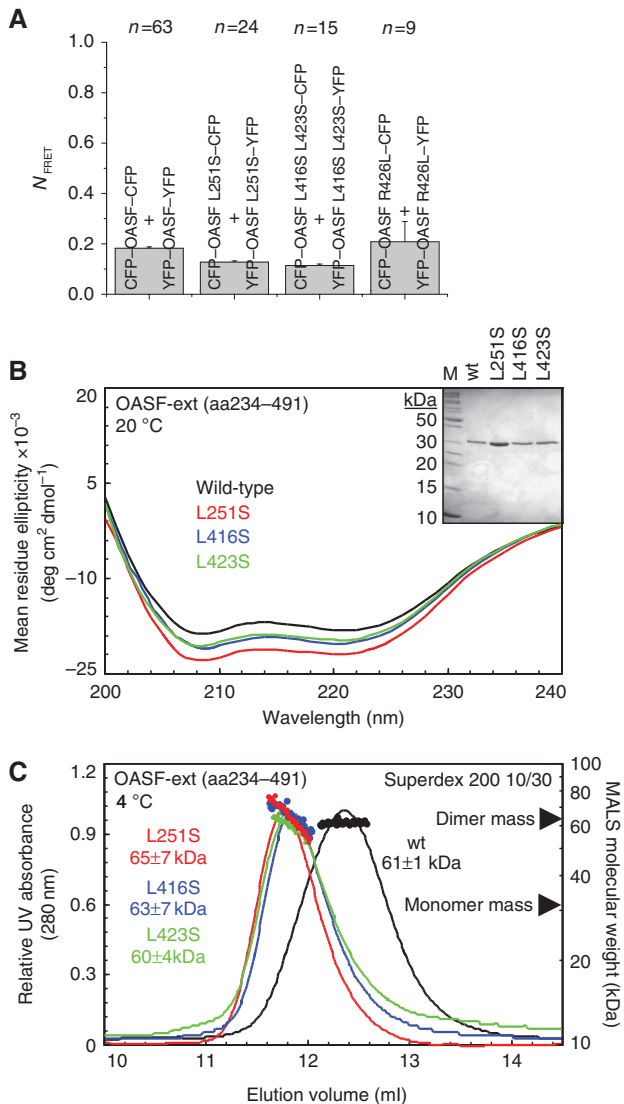
Figure 4 Dimerization/oligomerization and conformation of OASF and mutants. (**A**) Block diagram summarizing intermolecular NFRET between double-labelled CFP/CFP and YFP/YFP OASF forms: OASF (wild type), OASF L251S, OASF L416S L423S and OASF R426L. (**B**) Purity and far-UV CD spectra of OASF-ext (aa 234–491) mutant and wild-type forms. Spectra were acquired at 20°C in 20 mM Tris, 200 mM NaCl, 2 mM DTT, pH 8 using protein concentrations ranging from 0.14 to 0.35 mg ml^{-1}. Protein purity was confirmed using Coomassie-stained SDS–PAGE (inset). (**C**) SEC with in-line MALS analyses of OASF-ext (aa 234–491) mutant and wild-type forms. SEC experiments were performed at 4°C in 20 mM Tris, 100 mM NaCl, 50 mM L-Arg/L-Glu, 2 mM DTT, pH 8 using 0.85–2.0 mg ml^{-1} protein.

transition, all three mutant proteins exhibited a shorter elution time than the wild-type form in size exclusion chromatography (SEC) experiments (Figure 4C). The shorter elution times are not due to a significant change in quaternary structure, since the in-line multiangle light scattering (MALS) analyses suggested dimer molecular weights for mutant and wild-type proteins (Figure 4C). The shorter elution times suggested an extended conformation for the OASF-ext mutants compared with the wild-type form in line with the FRET measurements (Figure 3A).

Thus, based on our mutation data, all three coil-coiled regions within the cytosolic portion of STIM1 have a

role in mediating the intramolecular head-to-tail proximity of OASF.

Coupling of OASF mutants to ORAI1

A decreased YFP–OASF–CFP FRET might reflect an intramolecular transition to an extended conformation with a potential exposure of the CAD/SOAR domain. This concept was tested by co-expressing ORAI1 with L251S, A376K or L416/423S YFP–OASF–CFP mutants that exhibited the most pronounced reduction of FRET compared with the wild-type sensor in the absence of ORAI1. Co-expression of ORAI1 together with the L251S and L416/423S OASF mutants (Figure 3B) revealed clearly stronger membrane localization than that obtained with wild-type OASF sensor as evident from respective intensity profiles (Figure 3D). Hence, a more extended OASF conformation might allow for enhanced binding to ORAI1. The A376K OASF mutant behaved differently, however, exhibiting a reduced FRET but failing to interact with ORAI1 (Figure 3B–D). Previous studies focused on the second coiled-coil domain as a potential site for interaction with ORAI1 C-terminus (Frischauf *et al*, 2009; Calloway *et al*, 2010; Covington *et al*, 2010). This interaction may have been impaired by the A376K mutation despite the extended OASF conformation. The R426L OASF mutant failed to interact with ORAI1 (Figure 3C and D), suggesting that a sequentially more canonical third coiled-coil domain interfered with the extended conformation potentially required for coupling to ORAI1. Hence, mutations within the first and third coiled-coil domains designed to potentially destabilize intramolecular coiled-coil interactions promoted switching of OASF into an extended conformation, this in turn facilitated interaction with ORAI1 probably by enhanced exposure of the CAD/SOAR domain.

Coupling of OASF to ORAI1–R91W

The ORAI1–R91W mutant linked to SCID represents a nonfunctional CRAC channel due to a defect in gating/permeation rather than in interaction with full-length STIM1 (Navarro-Borelly *et al*, 2008; Derler *et al*, 2009). However, previous FRET microscopy studies show that while the STIM1–ORAI1–R91W interaction is preserved, it is somewhat attenuated (Muik *et al*, 2008). Surprisingly, co-expression of ORAI1–R91W with wild-type YFP–OASF–CFP revealed no clear evidence for an interaction (Figure 5A). On the other hand, the OASF L251S and L416/423S mutants that showed enhanced interaction with wild-type ORAI1 were capable of coupling to ORAI1–R91W (Figure 5B and C). As expected, they failed to induce an ORAI1–R91W current (data not shown), consistent with a profound ORAI1 gating defect. The density profiles of OASF L251S and L416/423S mutants co-expressed with ORAI1–R91W (Figure 5B and C) suggested a decrease in the affinity for their interaction when compared with profiles of the OASF mutants with wild-type ORAI1 (Figure 3D), consistent with the reduced but detectable interaction with full-length STIM1 (Derler *et al*, 2009). Hence, the ORAI1–R91W mutant appears deficient in the ability to switch OASF into its extended conformation via interaction. To evaluate the degree of this deficiency, we tested the V419S OASF mutant that showed only slight attenuation of FRET compared with wild-type OASF when expressed in the absence of ORAI1 (Supplementary Figure S4B). The V419S sensor mutant was indeed able to
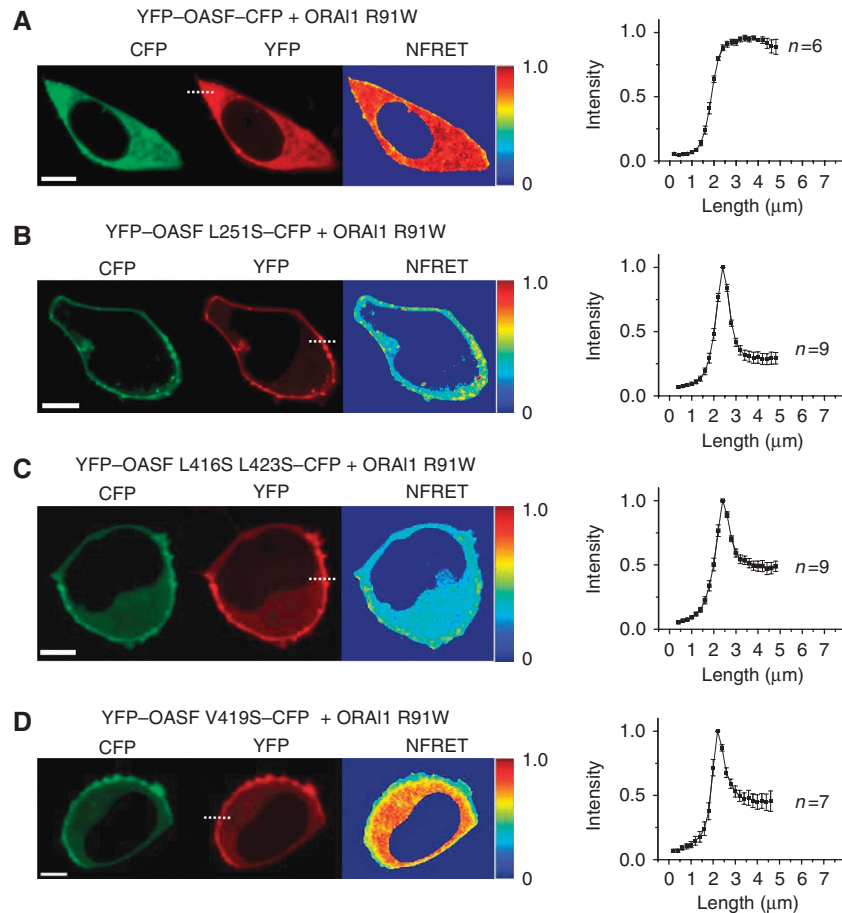
Figure 5 OASF sensor coupling to ORAI1–R91W. (Left panel) Localization and calculated NFRET life cell image series of HEK293 cells expressing ORAI1$_{R91W}$ and (**A**) YFP–OASF–CFP, (**B**) YFP–OASF L251S–CFP, (**C**) YFP–OASF L416S L423S–CFP, (**D**) YFP–OASF V419S–CFP. Calibration bar is 5 µm throughout. (Right panel) Corresponding intensity plots representing localization of YFP–OASF–CFP and mutants in regions close to the cell membrane as indicated by the dashed line.

interact with the ORAI1–R91W mutant, and this interaction was accompanied by a substantial decrease of FRET close to the plasma membrane (Figure 5D), consistent with full-length STIM1 observations (Muik *et al*, 2008; Derler *et al*, 2009). The ability of the ORAI1–R91W mutant to drive the V419S OASF mutant into a more extended conformation might imply that the intramolecular transition within OASF is coupled to the interaction with rather than the gating/permeation of ORAI1.

Mutations in full-length STIM1

To validate these findings derived from the OASF conformational sensor, we introduced some selected mutations within the full-length STIM1 (Figure 6) and an ER-located STIM1 fragment (aa 199–535; Supplementary Figure S6). The latter construct lacking the luminal N-terminal region and comprising only the ER membrane sequence (aa 199–232) together with the ERM domain (aa 233–535) allowed the elimination of store-dependent effects and the contribution of the polybasic cluster to puncta formation (Liou *et al*, 2007). While wild-type STIM1 (Figure 6A) only co-localized with and activated ORAI1 following store depletion by the Ca^{2+}-ATPase inhibitor 2,5′-di(tert-butyl)-1,4-benzohydroquinone (BHQ), both the L251S (Figure 6B) and L416/423S (Figure 6C) STIM1 mutants co-clustered with ORAI1 before

store depletion, leading to constitutive ORAI1-derived currents. Similarly, the ER-localized mutant STIM1 fragments (Supplementary Figure S6B, C and E) clustered with ORAI1, producing constitutive currents without store depletion. These inward currents were significantly reduced (Supplementary Figure S6E) or absent (Figure 6A) in experiments using the wild-type STIM1 forms.

Store depletion only slightly altered co-clustering of ORAI1 and full-length STIM1 with mutations introduced in the first or third coiled-coil domain. Hence, these STIM1 mutants without store depletion might have led to a conformational exposure of the ORAI1 interaction site(s) within the STIM1 C-terminal region thereby outweighing most of the inhibitory effect exerted by the full Ca^{2+} stores via the N-terminal region of STIM1. Further, the ER-located fragments with the L251S and the L416/423S coiled-coil mutations resulted in substantially more co-clustering with ORAI1 and larger ORAI1 currents compared with the wild-type form (Supplementary Figure S6). Consistent with R426L OASF that resisted a conformational transition, the R426L full-length STIM1 mutant (Figure 6D) and the corresponding ER-located mutant STIM1 fragment (Supplementary Figure S6D and E) exhibited minimal (Figure 6D) or lack of (Supplementary Figure S6D) co-clustering with ORAI1 after store depletion. Consequently, these constructs yielded only minor
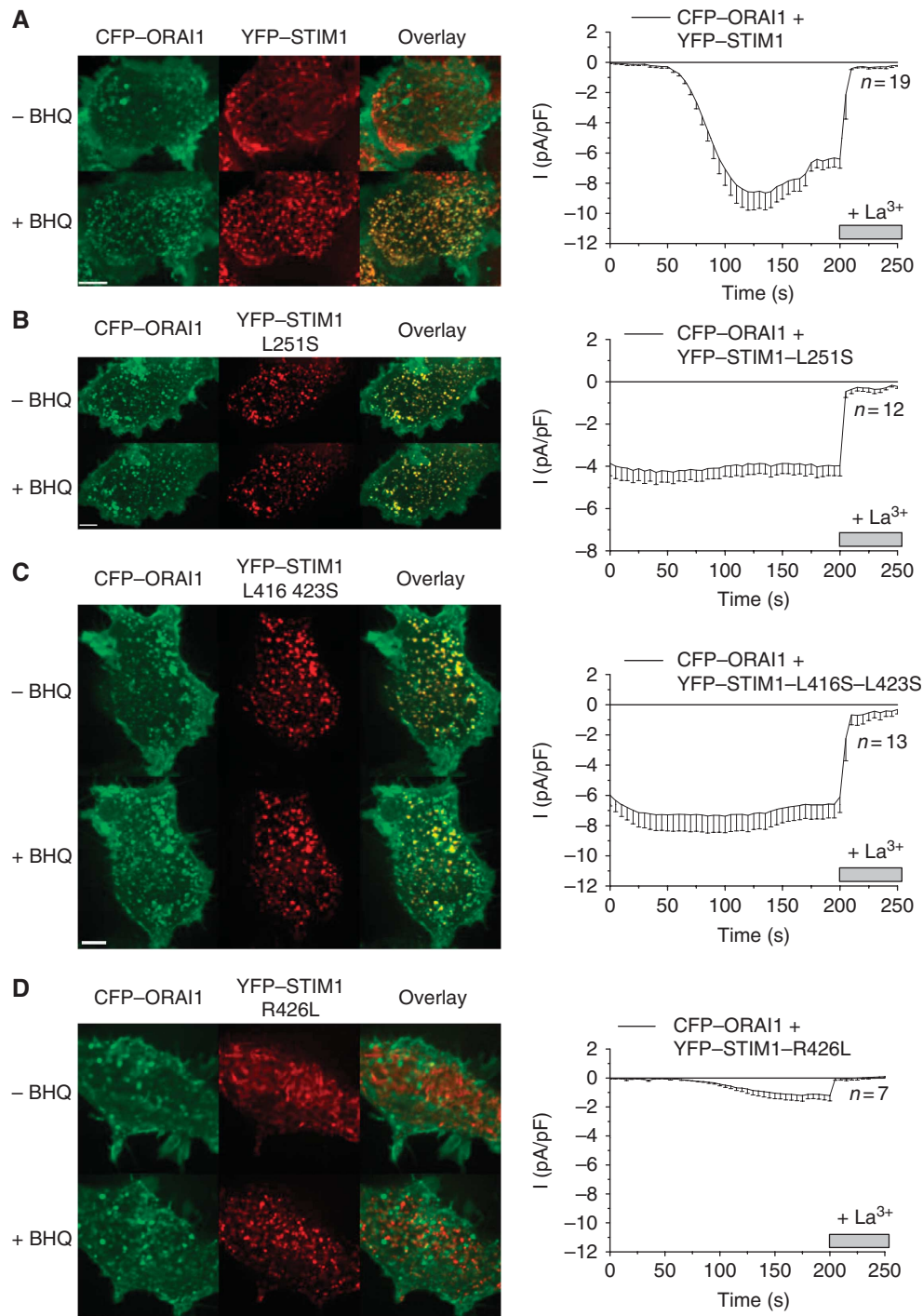
Figure 6 Controlling full-length STIM1 clustering and coupling efficiency with ORAI1. (Left panel) Life cell image series showing localization and overlay from HEK293 cells expressing CFP–ORAI1 and (**A**) YFP–STIM1, (**B**) YFP–STIM1 L251S (**C**) YFP–STIM1 L416S L423S (**D**) YFP–STIM1 R426L under resting cell conditions (upper panel) and following 5 min store depletion with 60 μM BHQ in nominally free extracellular Ca^{2+} solutions (lower panel). (Right panel) Respective time courses of whole-cell inward currents at −86 mV activated by passive store depletion and blocked by 10 μM La^{3+} at $t = 200$ s.

(Figure 6D) or no (Supplementary Figure S6E) ORAI1 currents. Noteworthy, the interaction as well as stimulatory capability of the R426L full-length STIM1 mutant on ORAI1 was much more impaired than its ability to form puncta in response to store depletion. Hence, STIM1 oligomerization is not sufficient for its conformational coupling with ORAI1 unless an extended C-terminal conformation is adopted.

STIM1-derived FRET sensor as tool for drug screening

We investigated whether the OASF conformational sensor might be utilized for screening of STIM1/ORAI1 as drug targets. As proof of principle, 2-APB was used, a powerful modifier of the STIM1/ORAI machinery with several, complex target sites. 2-APB stimulates ORAI3 channels (Lis *et al*, 2007; Schindl *et al*, 2008), disrupts STIM1 clusters (DeHaven *et al*, 2008; Peinelt *et al*, 2008; Tamarina *et al*, 2008) and

ORAI1–STIM1 complexes with canonical transient receptor potential channels or IP$_3$ receptors (Hong *et al*, 2011). In contrast, the C-terminus of STIM1 or a shorter fragment (aa 235–505) has been reported to rapidly associate with ORAI1 when 2-APB is administered (Wang *et al*, 2009). In our experiments, treatment of the OASF sensor with 75 μM 2-APB induced a slight FRET decrease, suggesting a conformational rearrangement towards an extended conformation (Supplementary Figure S7A and B). In the presence of ORAI1, the OASF sensor exhibited further redistribution close to the plasma membrane following 2-APB addition, together with a further decreased FRET (Supplementary Figure S7C and D). A similar 2-APB driven interaction of STIM1 C-terminal fragments with ORAI1 has previously been described as an ORAI1-mediated process, resulting in a current increase (Wang *et al*, 2009). Hence, the OASF sensor indeed allowed to detect an effect of 2-APB via FRET and suggested enhanced interaction of the slightly extended conformation of OASF as potential mechanism for strong coupling to and activation of ORAI1 currents. However, the OASF C-terminal fragment seems to behave distinct to the full-length STIM1 form where 2-APB exerts complex, distinct actions as previously mentioned.

Discussion

Here, we presented a STIM1-derived conformational sensor that allowed for probing of intramolecular transitions within its cytosolic domains. This region of STIM1 switched from a tight into an extended conformation either by interaction with ORAI1 or via mutations introduced in the first or third putative coiled-coil domain. These engineered STIM1 constructs with extended conformations exhibited an enhanced interaction with both wild-type and the SCID-linked R91W mutant ORAI1. The mutation-induced extended STIM1 C-terminal conformation reflects an intramolecular transition, which likely exposes the CAD/SOAR domain and promotes interaction of full-length STIM1 with ORAI1, even in the absence of store depletion. We suggest that these mutant full-length STIM1 proteins that interact with and constitutively activate ORAI1 channels imitate a physiological activated state, which mimics the conformational change that occurs in native STIM1 upon store depletion. The transition is mediated by a change in the intramolecular associations and/or orientations of the three putative coiled-coil domains within the STIM1 C-terminus.

CAD/SOAR (Park *et al*, 2009; Yuan *et al*, 2009) represents the minimal cytosolic region within STIM1 that is sufficient for its homomerization, interaction with and activation of ORAI1. It comprises the second (aa 364–389) and third (aa 399–423) coiled-coil domains together with an extended stretch (aa 423–448) contributing to homomerization (Muik *et al*, 2009). Here, we presented evidence that the OASF FRET sensor that encompasses the first coiled-coil region (aa 238–342) and the CAD/SOAR domain adopts a tight conformation that is extended upon coupling to ORAI1. As this required intact N- and C-termini of ORAI1 (Figures 2C and 5A), it is tempting to speculate that the extended conformation reflects bridging of OASF between ORAI1 cytosolic termini, which is facilitated by the OASF coiled-coil mutants (L251S, L416, 423S) pre-locked in the extended conformation. Accordingly, N-terminal deletions (Δ233–251) or the L251S

mutation located in the N-terminal region of the first putative coiled-coil domain set OASF in an extended conformation that promoted enhanced interaction with ORAI1. As the essential ORAI1-binding site within OASF is suggested within the second rather than the first coiled-coil domain (Frischauf *et al*, 2009; Calloway *et al*, 2010), these manipulations that locally disturbed the putative first coiled-coil structure of OASF probably removed its masking effect on the CAD/SOAR domain thereby facilitating an interaction with ORAI1. A similar phenomenon was observed with mutations within the third coiled-coil domain in that variations that locally destabilize (L416, 423S) or stabilize (R426L) the putative coiled-coil structure enhanced or attenuated coupling to ORAI1, respectively. Thus, the OASF conformation defined by the precise intramolecular coiled-coil arrangements regulates the affinity of STIM1:ORAI1 coupling requisite for channel gating.

We and others have recently provided data (Frischauf *et al*, 2009; Calloway *et al*, 2010) that suggest the second coiled-coil domain encompasses the potential interaction site for coupling to a putative coiled-coil domain on the C-terminus of ORAI1. Destabilizing the putative second coiled-coil domain by L373S and A376S as well as A376K mutations inhibited the interaction with ORAI1 (Frischauf *et al*, 2009; Covington *et al*, 2010), and switched OASF in an extended conformation.

Recently, data from the Balla laboratory (Korzeniowski *et al*, 2010) suggest a basic segment within the second coiled-coil domain to interact with an acidic cluster in the first coiled-coil region (see Supplementary Figure S3) in resting STIM1. Following store depletion, this interaction may be disrupted by an intramolecular switching mechanism that enables the basic segment in the second coiled coil of STIM1 to couple to acidic residues within the C-terminal coiled-coil domain of ORAI1 (Korzeniowski *et al*, 2010). The OASF FRET sensor presented here allowed for the first time measurement of the conformational change accompanying the intramolecular switch upon STIM1 C-terminus interaction with ORAI1. Introduction of neutralizing mutations (Korzeniowski *et al*, 2010) within the acidic cluster (E318/319/320/322A, =4EA) in the OASF FRET sensor significantly reduced FRET compatible with a decrease of the proposed intramolecular interaction with the basic segment (Supplementary Figure S4). In addition to the acidic cluster in the first coiled-coil region, we further identified hydrophobic amino acids in the first and the third coiled-coil domains that allowed for switching STIM1 C-terminal fragments from a tight into an extended conformation as determined by FRET and MALS. These mutations (L251S, L416S and L423S) introduced into full-length STIM1 apparently locked a physiologically active state resulting in co-clustering with and activation of ORAI1 currents without store depletion.

These observations suggest that the STIM1 C-terminal intramolecular transition is controlled by a complex interplay between the first, second and third coiled-coil domains, together controlling the exposure of CAD/SOAR domain and regulating the affinity of the potential ORAI1-interacting site. In a model combining Balla's work (Korzeniowski *et al*, 2010) and results from this study, we suggest that both hydrophobic as shown here together with electrostatic interactions contribute to the intramolecular coiled-coil transitions within the STIM1 C-terminal portion. In a straightforward scenario, oligomerization of STIM1 likely helps to

extend its C-terminal conformation controlled by domains within the first and third coiled-coil regions. Particularly, the R426L mutation in the latter that allowed for clustering of full-length STIM1 upon store depletion but failed to markedly interact with ORAI1 revealed the requisite for a balanced interplay culminating in CAD/SOAR exposure. The precise mechanism as to how oligomerization of STIM1 induced via store depletion (Luik *et al*, 2008) achieves this intramolecular transition requires further studies (Wang *et al*, 2010).

Our OASF conformational sensor additionally served as a sensitive tool to resolve deficiencies in the SCID-linked ORAI1–R91W mutant (Feske *et al*, 2006) aside from the profound gating defect. This non-functional ORAI1–R91W mutant, in contrast to wild-type ORAI1, was unable to interact with the OASF conformational sensor. While the latter was able to induce an extended OASF conformation, the R91W mutant could not promote the transition. Further, an interaction with the R91W mutant was only observed when the OASF sensor was in a slightly or fully extended form by mutation in the first or third coiled-coil domain. Thus, the ORAI1–R91W mutant has an attenuated ability to induce an extended STIM1 conformation. None of the interacting OASF mutants were able to recover the channel function of the ORAI1–R91W mutant consistent with a severe impairment of gating/permeation (Derler *et al*, 2009).

The OASF conformational sensor may be used to study the action of small molecules on the principal molecular components of SOC. For example, incubation of 2-APB with the OASF conformational sensor induced a slightly extended conformation reflected by a decrease of FRET. Thus, interaction of 2-APB with OASF might initiate an intramolecular transition that facilitates coupling with ORAI1, although the structural basis might be distinct to that obtained by coiled-coil mutations.

In conclusion, our STIM1-derived conformational sensor is applicable as a general tool not only for further dissecting the nature of STIM1 to ORAI1 coupling, but also for characterizing STIM1 interactions with drugs and other proteins such as CRACR2A (Srikanth *et al*, 2010) or the L-type Ca^{2+} channel (Park *et al*, 2010).

Materials and methods

Molecular cloning and mutagenesis
Human ORAI1 (ORAI1; accession number NM_032790) was kindly provided by A Rao's lab (Harvard Medical School). N-terminally tagged ORAI1 constructs were cloned via *Sal*I and *Sma*I restriction sites of pECFP-C1 and pEYFP-C1 expression vectors (Clontech) and C-terminally tagged ORAI1 constructs were cloned using the *Xho*I and *Bam*HI sites of the vectors pECFP-N1 and pEYFP-N1. All ORAI1 point mutants (R91W; E106Q; L273S) were produced using the QuikChange XL site-directed mutagenesis kit (Stratagene). For untagged ORAI1 constructs, stop codons were introduced in ORAI1–YFP, ORAI1–YFP–R91W, ORAI1–YFP–E106Q and ORAI1–YFP–L273S directly after the ORAI1-coding sequence.
Human STIM1 (STIM1; accession number NM_003156) N-terminally ECFP- and EYFP-tagged was kindly provided by T Meyer's Lab, Stanford University. For double-tagged STIM1 constructs, CFP was cloned into pEYFP-C2 via *Sac*II and Xba1 and the respective STIM1 fragments were introduced via *Eco*RI and *Sac*II (233–420, 233–430, 233–450, 233–474, 233–485, 233–535, 233–685). The same procedure was used for construction of YFP–233–474–YFP and CFP–233–474–CFP. All STIM1 point mutants (L251S; A376K, L416S L423S; R426L) were generated using the QuikChange XL site-directed mutagenesis kit (Stratagene).
The integrity of all resulting clones was confirmed by sequence analysis.

Electrophysiology and cell transfection
Cells transfected (Transfectin, Bio-Rad) with 1 µg DNA of ORAI1 and STIM1 constructs were identified by CFP/YFP fluorescence. Electrophysiological experiments were performed after 12–48 h, using the patch-clamp technique in whole-cell recording configurations at 21–25°C. For reducing cell density, cells were sometimes reseeded >7 h before the experiments started. An Ag/AgCl electrode was used as reference electrode. Voltage ramps were applied every 5 s from a holding potential of 0 mV, covering a range of −90 to 90 mV over 1 s. For passive store depletion the internal pipette solution included (in mM): 145 Cs methane sulphonate, 20 EGTA, 10 HEPES, 8 NaCl, 3.5 $MgCl_2$, pH 7.2. Standard extracellular solution consisted of 145 NaCl, 10 HEPES, 10 $CaCl_2$, 10 glucose, 5 CsCl, 1 $MgCl_2$, pH 7.4. A liquid junction correction of +12 mV resulted from a Cl^- based bath solution and a sulphonate-based pipette solution. Current traces were leak corrected by subtracting the remaining currents after 10 µM La^{3+} application at the end of the experiment.

Fluorescence microscopy
Confocal FRET microscopy was performed as previously described (Singh *et al*, 2006). In brief, a QLC100 Real-Time Confocal System (VisiTech Int., UK) was used for recording fluorescence images connected to two Photometrics CoolSNAPHQ monochrome cameras (Roper Scientific) and a dual port adapter (dichroic: 505lp; cyan emission filter: 485/30; yellow emission filter: 535/50; Chroma Technology Corp.). This system was attached to an Axiovert 200 M microscope (Zeiss, Germany) in conjunction with an argon ion multiwavelength (457, 488 and 514 nm) laser (Spectra Physics). The wavelengths were selected by an Acousto Optical Tuneable Filter (VisiTech Int., UK). Image acquisition and control of the confocal system was performed with MetaMorph 5.0 software (Universal Imaging Corp.). CFP, FRET and YFP images were typically illuminated over 900–1500 ms and consecutively recorded with a minimum delay. Image correction due to cross-talk and cross-excitation were performed prior to the calculation. Therefore, appropriate cross-talk calibration factors were determined for each construct on every day of the FRET experiment. After threshold determination and background subtraction, the corrected FRET image (N_{FRET}) was calculated on a pixel-to-pixel basis with a custom-made software (Derler *et al*, 2006) integrated in MatLab 7.0.4 according to the method published (Xia and Liu, 2001). The local CFP to YFP ratio might vary due to different localizations of diverse protein constructs, which could result in the calculation of false FRET values (Berney and Danuser, 2003). Accordingly, the analysis was limited to pixels with a CFP:YFP molar ratio within 1:10 to 10:1 to assure reliable results (Berney and Danuser, 2003).
Line-scans were extracted from individual images as indicated by the dashed lines with a total scan width of 25 pixels corresponding to a length of 5 µm. Intensity values along each individual scan were normalized to the highest value in the respective scan. Then, normalized line-scans were aligned for averaging either at the peak maximum or along the increasing slope representing the cell edge when no clear peak was present.

Cloning and recombinant expression of OASF-ext
Human STIM1 cDNA was from Origene (Origene Technologies, Inc). The cytosolic region encompassing residues Asn234 to Gln491 (aa 234–491) was subcloned into a pET-28a vector (Novagen, Inc.) and expressed with an N-terminal His_6-tag in BL21(DE3) *E. coli* cells. The protein was extracted out of inclusions using guanidine, isolated using Ni-NTA resin (Qiagen, Inc.) and refolded into 20 mM Tris, 100 mM NaCl, 50 mM L-Arg/L-Glu, 2 mM DTT (pH 8). After thrombin digestion of the His_6-tag, the protein was further purified by SEC on a Superdex 200 PG 10/60 column. The identity of the protein was confirmed by positive electrospray ionization mass spectrometry. Protein concentration was estimated using $\varepsilon_{280\,nm} = 0.95$ $(mg\,ml^{-1})^{-1}\,cm^{-1}$.

Far-UV CD
Far-UV CD spectra were recorded on a Jasco J-815 CD Spectrometer (Jasco, Inc.). Data were collected in 1 nm increments using 0.1 cm ES quartz cuvette pathlengths. Wavelength scan rates were at 20 nm per minute, with a response time of 8 s and bandwidth of 1 nm at each wavelength. Thermal melts were acquired in 1°C increments at a scan rate of 1°C per minute, with a response time of 8 s at each

temperature through 0.1–0.2 cm pathlengths. Protein concentration ranged from 0.14 to 0.35 mg ml^{-1}.

Analytical SEC with MALS

SEC was performed on Superdex 200 10/300 GL columns (GE Healthcare Biosciences Corp.) at 4°C. MALS analyses were performed in-line, using the three angle (45°, 90° and 135°) miniDawn static light scattering instrument with a 690-nm laser (Wyatt Technologies, Inc.) and an Optilab rEX differential refractometer (Wyatt Technologies, Inc.). Molecular weight was calculated from the ASTRA software (Wyatt Technologies, Inc.) based on Zimm plot analysis using a dn dc^{-1} = 0.1851 g^{-1}.

Western blot

HEK cells transiently transfected with YFP–OASF–CFP were lysed with 1 ml high salt lysis buffer (20 mM Tris/100 mM NaCl/2 mM EDTA/10% glycerol/1% nonidet P-40/protease inhibitor cocktail). After centrifugation, supernatants were mixed with laemmli buffer and lysates were separated by 10% SDS–PAGE. After western blotting, Y–OASF–C was detected by an anti-GFP antibody (Roche) and the correct size of the protein (YFP/CFP-tags: ∼26 kDa, OASF: ∼27 kDa) was verified by a suitable protein Standard (Bio-Rad).

Supplementary data

Supplementary data are available at *The EMBO Journal* Online (http://www.embojournal.org).

Acknowledgements

Conflict of interest

The authors declare that they have no conflict of interest.

References

Baba Y, Hayashi K, Fujii Y, Mizushima A, Watarai H, Wakamori M, Numaga T, Mori Y, Iino M, Hikida M, Kurosaki T (2006) Coupling of STIM1 to store-operated Ca2 + entry through its constitutive and inducible movement in the endoplasmic reticulum. *Proc Natl Acad Sci USA* **103:** 16704–16709

Barr VA, Bernot KM, Srikanth S, Gwack Y, Balagopalan L, Regan CK, Helman DJ, Sommers CL, Oh-Hora M, Rao A, Samelson LE (2008) Dynamic movement of the calcium sensor STIM1 and the calcium channel Orai1 in activated T-cells: Puncta and Distal caps. *Mol Biol Cell* **19:** 2802–2817

Berney C, Danuser G (2003) FRET or no FRET: a quantitative comparison. *Biophys J* **84:** 3992–4010

Berridge MJ, Bootman MD, Roderick HL (2003) Calcium signalling: dynamics, homeostasis and remodelling. *Nat Rev Mol Cell Biol* **4:** 517–529

Calloway NT, Holowka DA, Baird BA (2010) A basic sequence in STIM1 promotes Ca2 + influx by interacting with the C-terminal acidic coiled-coil of Orai1. *Biochemistry* **49:** 1067–1071

Covington ED, Wu MM, Lewis RS (2010) Essential role for the CRAC activation domain in store-dependent oligomerization of STIM1. *Mol Biol Cell* **21:** 1897–1907

DeHaven WI, Smyth JT, Boyles RR, Bird GS, Putney Jr JW (2008) Complex actions of 2-aminoethyldiphenyl borate on store-operated calcium entry. *J Biol Chem* **283:** 19265–19273

Derler I, Fahrner M, Carugo O, Muik M, Bergsmann J, Schindl R, Frischauf I, Eshaghi S, Romanin C (2009) Increased hydrophobicity at the N terminus/membrane interface impairs gating of the severe combined immunodeficiency-related ORAI1 mutant. *J Biol Chem* **284:** 15903–15915

Derler I, Hofbauer M, Kahr H, Fritsch R, Muik M, Kepplinger K, Hack ME, Moritz S, Schindl R, Groschner K, Romanin C (2006) Dynamic but not constitutive association of calmodulin with rat TRPV6 channels enables fine tuning of Ca2 + -dependent inactivation. *J Physiol* **577:** 31–44

Feske S (2007) Calcium signalling in lymphocyte activation and disease. *Nat Rev Immunol* **7:** 690–702

Feske S, Gwack Y, Prakriya M, Srikanth S, Puppel SH, Tanasa B, Hogan PG, Lewis RS, Daly M, Rao A (2006) A mutation in Orai1 causes immune deficiency by abrogating CRAC channel function. *Nature* **441:** 179–185

Finn BE, Evenas J, Drakenberg T, Waltho JP, Thulin E, Forsen S (1995) Calcium-induced structural changes and domain autonomy in calmodulin. *Nat Struct Biol* **2:** 777–783

Frischauf I, Muik M, Derler I, Bergsmann J, Fahrner M, Schindl R, Groschner K, Romanin C (2009) Molecular determinants of the coupling between STIM1 and Orai channels: differential activation of Orai1-3 channels by a STIM1 coiled-coil mutant. *J Biol Chem* **284:** 21696–21706

Grigoryan G, Keating AE (2008) Structural specificity in coiled-coil interactions. *Curr Opin Struct Biol* **18:** 477–483

Gruber M, Soding J, Lupas AN (2006) Comparative analysis of coiled-coil prediction methods. *J Struct Biol* **155:** 140–145

Hogan PG, Lewis RS, Rao A (2010) Molecular basis of calcium signaling in lymphocytes: STIM and ORAI. *Annu Rev Immunol* **28:** 491–533

Hong JH, Li Q, Kim MS, Shin DM, Feske S, Birnbaumer L, Cheng KT, Ambudkar IS, Muallem S (2011) Polarized but differential localization and recruitment of STIM1, Orai1 and TRPC channels in secretory cells. *Traffic* **12:** 232–245

Hoth M, Penner R (1992) Depletion of intracellular calcium stores activates a calcium current in mast cells. *Nature* **355:** 353–356

Huang GN, Zeng W, Kim JY, Yuan JP, Han L, Muallem S, Worley PF (2006) STIM1 carboxyl-terminus activates native SOC, I(crac) and TRPC1 channels. *Nat Cell Biol* **8:** 1003–1010

Korzeniowski MK, Manjarres IM, Varnai P, Balla T (2010) Activation of STIM1-Orai1 involves an intramolecular switching mechanism. *Sci Signal* **3:** ra82

Liou J, Fivaz M, Inoue T, Meyer T (2007) Live-cell imaging reveals sequential oligomerization and local plasma membrane targeting of stromal interaction molecule 1 after Ca2 + store depletion. *Proc Natl Acad Sci USA* **104:** 9301–9306

Liou J, Kim ML, Heo WD, Jones JT, Myers JW, Ferrell Jr JE, Meyer T (2005) STIM is a Ca2 + sensor essential for Ca2 + -store-depletion-triggered Ca2 + influx. *Curr Biol* **15:** 1235–1241

Lis A, Peinelt C, Beck A, Parvez S, Monteilh-Zoller M, Fleig A, Penner R (2007) CRACM1, CRACM2, and CRACM3 are store-operated Ca2 + channels with distinct functional properties. *Curr Biol* **17:** 794–800

Luik RM, Wang B, Prakriya M, Wu MM, Lewis RS (2008) Oligomerization of STIM1 couples ER calcium depletion to CRAC channel activation. *Nature* **454:** 538–542

Luik RM, Wu MM, Buchanan J, Lewis RS (2006) The elementary unit of store-operated Ca2 + entry: local activation of CRAC channels by STIM1 at ER-plasma membrane junctions. *J Cell Biol* **174:** 815–825

Martin SR, Bayley PM (1986) The effects of Ca2 + and Cd2 + on the secondary and tertiary structure of bovine testis calmodulin. A circular-dichroism study. *Biochem J* **238:** 485–490

Mercer JC, Dehaven WI, Smyth JT, Wedel B, Boyles RR, Bird GS, Putney Jr JW (2006) Large store-operated calcium selective currents due to co-expression of Orai1 or Orai2 with the intracellular calcium sensor, Stim1. *J Biol Chem* **281:** 24979–24990

Muik M, Fahrner M, Derler I, Schindl R, Bergsmann J, Frischauf I, Groschner K, Romanin C (2009) A cytosolic homomerization and a modulatory domain within STIM1 C terminus determine coupling to ORAI1 channels. *J Biol Chem* **284:** 8421–8426

Muik M, Frischauf I, Derler I, Fahrner M, Bergsmann J, Eder P, Schindl R, Hesch C, Polzinger B, Fritsch R, Kahr H, Madl J, Gruber H, Groschner K, Romanin C (2008) Dynamic coupling of

the putative coiled-coil domain of ORAI1 with STIM1 mediates ORAI1 channel activation. *J Biol Chem* **283:** 8014–8022

Navarro-Borelly L, Somasundaram A, Yamashita M, Ren D, Miller RJ, Prakriya M (2008) STIM1-Orai1 interactions and Orai1 conformational changes revealed by live-cell FRET microscopy. *J Physiol* **586:** 5383–5401

Oh-hora M, Rao A (2008) Calcium signaling in lymphocytes. *Curr Opin Immunol* **20:** 250–258

Parekh AB, Putney Jr JW (2005) Store-operated calcium channels. *Physiol Rev* **85:** 757–810

Park CY, Hoover PJ, Mullins FM, Bachhawat P, Covington ED, Raunser S, Walz T, Garcia KC, Dolmetsch RE, Lewis RS (2009) STIM1 clusters and activates CRAC channels via direct binding of a cytosolic domain to Orai1. *Cell* **136:** 876–890

Park CY, Shcheglovitov A, Dolmetsch R (2010) The CRAC channel activator STIM1 binds and inhibits L-type voltage-gated calcium channels. *Science* **330:** 101–105

Parry DA, Fraser RD, Squire JM (2008) Fifty years of coiled-coils and alpha-helical bundles: a close relationship between sequence and structure. *J Struct Biol* **163:** 258–269

Peinelt C, Lis A, Beck A, Fleig A, Penner R (2008) 2-Aminoethoxydiphenyl borate directly facilitates and indirectly inhibits STIM1-dependent gating of CRAC channels. *J Physiol* **586:** 3061–3073

Prakriya M, Feske S, Gwack Y, Srikanth S, Rao A, Hogan PG (2006) Orai1 is an essential pore subunit of the CRAC channel. *Nature* **443:** 230–233

Roos J, DiGregorio PJ, Yeromin AV, Ohlsen K, Lioudyno M, Zhang S, Safrina O, Kozak JA, Wagner SL, Cahalan MD, Velicelebi G, Stauderman KA (2005) STIM1, an essential and conserved component of store-operated Ca2 + channel function. *J Cell Biol* **169:** 435–445

Schindl R, Bergsmann J, Frischauf I, Derler I, Fahrner M, Muik M, Fritsch R, Groschner K, Romanin C (2008) 2-aminoethoxydiphenyl borate alters selectivity of Orai3 channels by increasing their pore size. *J Biol Chem* **283:** 20261–20267

Singh A, Hamedinger D, Hoda JC, Gebhart M, Koschak A, Romanin C, Striessnig J (2006) C-terminal modulator controls Ca2 + -dependent gating of Ca(v)1.4 L-type Ca2 + channels. *Nat Neurosci* **9:** 1108–1116

Smyth JT, Dehaven WI, Jones BF, Mercer JC, Trebak M, Vazquez G, Putney Jr JW (2006) Emerging perspectives in store-operated Ca2 + entry: roles of Orai, Stim and TRP. *Biochim Biophys Acta* **1763:** 1147–1160

Soboloff J, Spassova MA, Hewavitharana T, He LP, Xu W, Johnstone LS, Dziadek MA, Gill DL (2006) STIM2 is an inhibitor of STIM1-mediated store-operated Ca(2 +) entry. *Curr Biol* **16:** 1465–1470

Srikanth S, Jung HJ, Kim KD, Souda P, Whitelegge J, Gwack Y (2010) A novel EF-hand protein, CRACR2A, is a cytosolic Ca2 + sensor that stabilizes CRAC channels in T cells. *Nat Cell Biol* **12:** 436–446

Stathopulos PB, Zheng L, Ikura M (2009) Stromal interaction molecule (STIM) 1 and STIM2 calcium sensing regions exhibit distinct unfolding and oligomerization kinetics. *J Biol Chem* **284:** 728–732

Stathopulos PB, Zheng L, Li GY, Plevin MJ, Ikura M (2008) Structural and mechanistic insights into STIM1-mediated initiation of store-operated calcium entry. *Cell* **135:** 110–122

Steinmetz MO, Jelesarov I, Matousek WM, Honnappa S, Jahnke W, Missimer JH, Frank S, Alexandrescu AT, Kammerer RA (2007) Molecular basis of coiled-coil formation. *Proc Natl Acad Sci USA* **104:** 7062–7067

Tamarina NA, Kuznetsov A, Philipson LH (2008) Reversible translocation of EYFP-tagged STIM1 is coupled to calcium influx in insulin secreting beta-cells. *Cell Calcium* **44:** 533–544

Vig M, Beck A, Billingsley JM, Lis A, Parvez S, Peinelt C, Koomoa DL, Soboloff J, Gill DL, Fleig A, Kinet JP, Penner R (2006a) CRACM1 multimers form the ion-selective pore of the CRAC channel. *Curr Biol* **16:** 2073–2079

Vig M, Peinelt C, Beck A, Koomoa DL, Rabah D, Koblan-Huberson M, Kraft S, Turner H, Fleig A, Penner R, Kinet JP (2006b) CRACM1 is a plasma membrane protein essential for store-operated Ca2 + entry. *Science* **312:** 1220–1223

Wang Y, Deng X, Gill DL (2010) Calcium signaling by STIM and Orai: intimate coupling details revealed. *Sci Signal* **3:** pe42

Wang Y, Deng X, Zhou Y, Hendron E, Mancarella S, Ritchie MF, Tang XD, Baba Y, Kurosaki T, Mori Y, Soboloff J, Gill DL (2009) STIM protein coupling in the activation of Orai channels. *Proc Natl Acad Sci USA* **106:** 7391–7396

Woolfson DN (2005) The design of coiled-coil structures and assemblies. *Adv Protein Chem* **70:** 79–112

Wu MM, Buchanan J, Luik RM, Lewis RS (2006) Ca2 + store depletion causes STIM1 to accumulate in ER regions closely associated with the plasma membrane. *J Cell Biol* **174:** 803–813

Xia Z, Liu Y (2001) Reliable and global measurement of fluorescence resonance energy transfer using fluorescence microscopes. *Biophys J* **81:** 2395–2402

Xu P, Lu J, Li Z, Yu X, Chen L, Xu T (2006) Aggregation of STIM1 underneath the plasma membrane induces clustering of Orai1. *Biochem Biophys Res Commun* **350:** 969–976

Yeromin AV, Zhang SL, Jiang W, Yu Y, Safrina O, Cahalan MD (2006) Molecular identification of the CRAC channel by altered ion selectivity in a mutant of Orai. *Nature* **443:** 226–229

Yuan JP, Zeng W, Dorwart MR, Choi YJ, Worley PF, Muallem S (2009) SOAR and the polybasic STIM1 domains gate and regulate Orai channels. *Nat Cell Biol* **11:** 337–343

Zhang SL, Kozak JA, Jiang W, Yeromin AV, Chen J, Yu Y, Penna A, Shen W, Chi V, Cahalan MD (2008) Store-dependent and -independent modes regulating Ca2 + release-activated Ca2 + channel activity of human Orai1 and Orai3. *J Biol Chem* **283:** 17662–17671

Zhang SL, Yeromin AV, Zhang XH, Yu Y, Safrina O, Penna A, Roos J, Stauderman KA, Cahalan MD (2006) Genome-wide RNAi screen of Ca(2 +) influx identifies genes that regulate Ca(2 +) release-activated Ca(2 +) channel activity. *Proc Natl Acad Sci USA* **103:** 9357–9362

Zhang SL, Yu Y, Roos J, Kozak JA, Deerinck TJ, Ellisman MH, Stauderman KA, Cahalan MD (2005) STIM1 is a Ca2 + sensor that activates CRAC channels and migrates from the Ca2 + store to the plasma membrane. *Nature* **437:** 902–905